유연인쇄전자학술지, 2025년 6월, 제4권 제1호, pp. 109-123
Journal of Flexible & Printed Electronics, June 2025, Vol. 4, Issue 1, pp. 109-123
Received 2025-05-30, Revised 2025-06-16, Accepted 2025-06-18
https://doi.org/10.56767/jfpe.2025.4.1.109
eISSN: 2951-2174

RESEARCH

Anionic Conjugated Polyelectrolyte as a Multifunctional Interfacial Layer for Defect Suppression in Perovskite LEDs

Bum Chan Park[1], Rahmatia Fitri Binti Nasrun[2], Jihoon Kim[1], Dong Hwan Son[2], Hyun-Seock Yang[1*], Joo Hyun Kim[2*], Bo Ram Lee[1*]

[1]Department of Advanced Materials Science and Engineering, Sungkyunkwan University, Suwon, Korea
[2]Department of Polymer Engineering, Pukyong National University, Busan, Korea

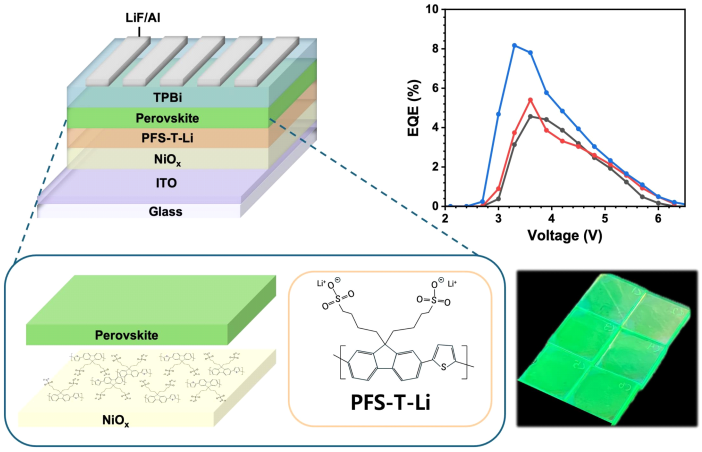

ABSTRACT

Nickel oxide (NiO_x) is widely used as a hole transport layer in perovskite light-emitting diodes (PeLEDs) due to its suitable energy level alignment, high transparency, and stability. However, its surface typically contains inhomogeneous oxygen vacancies and abundant hydroxyl groups, leading to interfacial energy mismatches and defect formation that hinder efficient charge injection and limit device performance. To address these challenges, we introduce a dual-passivation strategy employing an anionic conjugated polyelectrolyte (CPE), Poly[9,9-bis(4-C-sulfonatobutyl)fluorene-alt-thiophene]-Li (PFS-T-Li), as a multifunctional interfacial layer. The sulfonate groups (SO_3^-) and Li^+ counterions in PFS-T-Li selectively coordinate with oxygen vacancies in NiO_x and Pb^{2+}-related trap sites in the perovskite layer, respectively. This dual interfacial passivation effectively suppresses trap-assisted non-radiative recombination, enhancing charge injection, luminescence efficiency, and operational stability. Devices incorporating PFS-T-Li achieve a maximum external quantum efficiency (EQE) of 8.16 % and luminance of 5,111 cd m^{-2}, demonstrating its critical role in improving PeLED performance.

Key Words: Anionic conjugated polyelectrolyte, Multifunctional interfacial layer, Defect suppression, Perovskite light-emitting diodes

*Correspondence: randaifne@skku.edu, jkim@pknu.ac.kr, brlee@skku.edu

1. INTRODUCTION

Metal halide perovskites have attracted significant attention as next-generation optoelectronic materials owing to their exceptional optical properties, including excellent light-emitting characteristics, narrow full width at half maximum (FWHM), and tunable bandgaps [1-8]. These attributes have driven the rapid development of perovskite light-emitting diodes (PeLEDs), underscoring their technological promise in advanced display applications [9-15].

Despite these advantages, PeLEDs still face substantial stability challenges when exposed to external stimuli such as heat, moisture, and oxygen [16-21]. These limitations originate not only from intrinsic instabilities within the emissive perovskite layer but also from insufficient interfacial compatibility among the various functional layers that constitute the device architecture [22]. Therefore, achieving precise control over the physicochemical properties of all interfaces-particularly the hole transport layer (HTL)-is essential for realizing reliable and high-performance PeLEDs [23,24].

Nickel oxide (NiO_x) has emerged as a promising hole transport layer owing to its suitable energy level alignment, high optical transparency, and excellent thermal and chemical stability, even under humid and oxidative conditions [25-27]. However, the surface of NiO_x typically exhibits inhomogeneous oxygen vacancies and abundant hydroxyl groups (−OH), which induce interfacial charge asymmetry [28-29]. This results in a surface energy mismatch with the perovskite precursor solution, leading to poor film uniformity, increased interfacial defect density, and ultimately, enhanced non-radiative recombination that constrains device performance [30,31].

A widely adopted strategy to mitigate these interfacial issues involves coating poly (9-vinylcarbazole) (PVK) on NiO_x to improve wettability and chemical compatibility [29,32,33]. However, PVK, as a non-polar conjugated polymer, lacks intrinsic molecular polarity, resulting in weak electrostatic interactions and poor adhesion with the ionically polar NiO_x and perovskite layers. This polarity mismatch causes surface energy discrepancies that hinder uniform perovskite film formation and promote the formation of interfacial defects.

To overcome these limitations, this study introduces an anionic conjugated polyelectrolyte (CPE), poly [9,9-bis(4-C-sulfonatobutyl)fluorene-alt-thiophene]-Li (PFS-T-Li), as a multifunctional interfacial layer capable of enabling dual passivation at both the NiO_x and perovskite interfaces [34-39]. Featuring a conjugated backbone composed of fluorene and thiophene units, PFS-T-Li offers a delocalized π-electron transport pathway that facilitates efficient hole transport. Simultaneously, its sulfonate side chains (SO_3^-) and Li^+ counterions selectively coordinate with oxygen vacancies in NiO_x and Pb^{2+}-related trap sites in the perovskite layer, respectively, thereby enabling effective defect passivation and suppressing trap-assisted non-radiative recombination [40-42].

Moreover, the hydrophilic and ionic nature of PFS-T-Li alleviates the surface energy mismatch between NiO_x and the perovskite precursor solution, promoting uniform film formation and enhancing interfacial adhesion. By concurrently improving interfacial electronic stability and enabling efficient hole in-

jection, this dual-passivation strategy addresses critical interfacial challenges in PeLED fabrication. Consequently, this study demonstrates that the incorporation of PFS-T-Li represents an effective approach to enhance interfacial compatibility, suppress defect formation, and improve overall PeLED device performance.

2. METHODS

2.1. Materials

Nickel acetate tetrahydrate (98.0%), ethanol (95.0%), ethanolamine (99.5%), methanol (99.9%), cesium bromide (99.99%), PVK (Mw=1,100,000 g mol^{-1}), chlorobenzene (CB; 99.8%), 18-Crown-6 ether (Crown;≥ 99.0%), dimethyl sulfoxide (DMSO; 99.9%) 2,7-dibromofluorene (97.0%), potassium hydroxide (90.0%), tetrabutylammonium bromide (98.0%), tetraethylammonium hydroxide aqueous solution (20wt%) and lithium perchlorate (95.0%) were purchased from Sigma-Aldrich, n-Butylammonium bromide (BABr; 99.9%) was purchased from Greatcell Solar Materials. Lead bromide ($PbBr_2$≥98.0%) was purchased from Tokyo Chemical Industry (TCI). 2,2',2"-(1,3,5-benzinetriyl) tris(1-phenyl-1-H-benzimidazole) (TPBi, 99.9%) was purchased from OSM. Lithium fluoride (LiF, 99.9%) was purchased from iTASCO. and 1,4-butanesultone (99.0%), thiophene-2,5-diboronic acid bis(pinacol) ester (97%), tetrakis(triphenylphosphine) palladium (99.9%), were purchased from Fisher Scientific.

2.2. Device Fabrication

The Green quasi-2D PeLEDs were fabricated on an ITO substrate with three different HTL configurations. Device architectures are (1) ITO/ NiO_x/quasi-2D perovskite/TPBi/LiF/Al. (2) ITO/ NiO_x /PVK/quasi-2D perovskite/TPBi/LiF/Al. (3) ITO/NiO_x/PFS-Li/quasi-2D perovskite/TPBi/LiF/Al. The ITO substrates were treated with O_2 plasma for 30 minutes. For the preparation of NiO_x precursor solution, Nickel acetate tetrahydrate (99.5 mg) was dissolved in ethanol (4 mL) with ethanolamine (24.2 μL) and stirred for 4 hours. The NiO_x solution was spin coated on ITO at 4,000 rpm for 40 seconds and annealed at 300℃ on hotplate for 1 hour. After annealed, the substrates were transferred into a N2-filled glove box. For NiO_x/PVK-based devices, a PVK (4 mg mL^{-1} in CB) solution was spin-coated onto the NiO_x layer at 4,000 rpm for 40 seconds and annealed at 130℃ for 10 minutes.

The synthesis of PFS-T-Li was carried out in three steps. First, compound 1 was synthesized by reacting 2,7-dibromofluorene (3.00 mmol, 0.97 g), tetrabutylammonium bromide (0.30 mmol, 96.7 mg), and potassium hydroxide (50 wt%, 5 mL) in DMSO (30 mL) under nitrogen. After stirring at 60℃ for 30 min, 1,4-butanesultone (6.60 mmol) was added and the reaction was continued at 60℃ for 24 h. The resulting mixture was precipitated in acetone and purified by washing with diethyl ether, followed by recrystallization in ethanol to obtain compound 1 (1.61 g, 80%).

Second, compound 1 (0.4 mmol) was polymerized with thiophene-2,5-diboronic acid bis (pinacol) ester (0.4 mmol) using tetrakis (triphenylphosphine)palladium (0) (10 mol%) as the catalyst in a mixture of degassed DMF (3 mL) and aqueous tetraethylammonium hydroxide solution (20%, 3 mL). The reaction was performed at 95℃ for 48 h under nitrogen. The resulting polymer (PFS-T) was purified by dialysis, yielding

83%.

Finally, ion exchange was performed to obtain the lithium form of the polymer. PFS-T was dissolved in methanol and reacted with lithium perchlorate (20 equivalents) at room temperature for 24 h. The polymer was then purified by dialysis to afford PFS-T-Li with a 90% yield. For PFS-T-Li-based devices, a PFS-T-Li solution (0.3 mg mL^{-1} in methanol) was spin-coated under the same condition (4,000 rpm, 40 seconds) and annealed at 120℃ for 15 minutes.

For PFS-T-Li-based devices, a PFS-T-Li solution (0.3 mg mL^{-1} in methanol) was spin-coated under the same condition (4,000 rpm, 40 seconds) and annealed at 120℃ for 15 minutes.

For the NiO_x-based devices, no additional layer was deposited on top of the - film. Subsequently, 0.25 M perovskite precursor solution containing $PbBr_2$, CsBr, and BABr in a molar ratio of 1:0.9:1.2 was prepared in 1 mL DMSO with 4 mg of 18-crown-6. quasi-2D perovskite precursor solution spin coated on each HTLs 500 rpm for 5 seconds and 5,000 rpm for 40 seconds and annealed 120℃ for 5 minutes. Finally, TPBi (75 nm), LiF (2 nm), Al (100 nm) was deposited via thermal evaporator in 5×10^{-6} torr.

2.3. Characterizations

The work function values of ITO, ITO/NiO_x, ITO/NiO_x/PVK, and ITO/NiO_x/PFS-T-Li were determined using Kelvin probe microscopy (KPM, KP Technology Ltd., Model KP020). The contact potential difference (CPD) between each sample and the KPM tip was measured to estimate their respective work functions. Prior to measurement, the KPM tip was calibrated using a reference gold surface with a known work function of 5.1 eV. The surface roughness was measured by atomic force microscopy (XE-100, Park System) in contact mode. XPS analysis was determined using a KRATOS Analytical Ltd. (AXIS SUPRA). The PLQY was measured by an absolute photoluminescence quantum yield spectrometer (Quantaurus-QY) from HAMAMATSU with excitation wavelength of 375 nm. UV visible spectra of thin films were determined using a JASCO V-730. The *J*–*V*, *L*–*V*, *EQE*-*V* curves, and electroluminescence features were measured by a Keithley 2,450 source meter with a CS2000 spectroradiometer (Konica Minolta) in a N_2 filled glovebox.

3. RESULTS AND DISCUSSION

Fig. 1(a) illustrates the chemical structure of CPE, PFS-T-Li, which was designed to function as a multifunctional interfacial layer in PeLEDs. This polymer features a π-conjugated backbone composed of fluorene and thiophene units, providing an extended delocalized π-electron pathway to support hole transport. In particular, in case of thiophene, a planar heteroaromatic ring with high electron density, enhances the π-conjugation between adjacent fluorene units, thereby promoting charge delocalization [35].

Anionic sulfonate groups (SO_3^-) are introduced into the side chains and are intended to provide strong electrostatic and coordination interactions at the interface, facilitating robust binding with both NiO_x and the perovskite layer. The sulfonyl moieties also allow for charge delocalization, which is expected to stabilize counterions such as Li^+. Based on this design, PFS-T-Li is anticipated to exert a dual-passivation effect by targeting oxygen vacancies on the NiO_x surface and

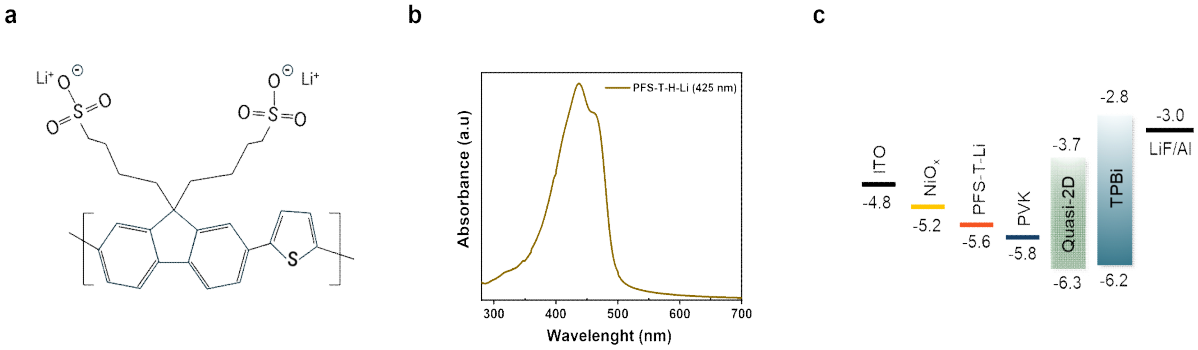

Fig. 1. (a) The chemical structure of PFS-T-Li. (b) Ultraviolet (UV) – visible absorption spectra of PFS-T-Li thin film. (c) Energy level diagram of PeLED device.

undercoordinated Pb^{2+} defects in the perovskite layer.

Leveraging this molecular architecture, PFS-T-Li is intended to act as a multifunctional interfacial layer that enhances hole injection from NiO_x to the perovskite by modulating interfacial energy alignment, regulating charge distribution, and passivating interfacial trap states.

In the UV-Vis absorption spectrum, PFS-T-Li exhibits a distinct π-π* transition peak at approximately 425 nm (Fig. 1(b)), attributed to the π-conjugated structure along the polymer backbone, supporting its light-absorbing characteristics as a conjugated polyelectrolyte. This absorption wavelength shows minimal overlap with the emission range of the perovskite layer (510−520 nm), thereby minimizing optical loss upon interfacial insertion. To examine interfacial energetics, the contact potential differences (CPD) of each HTL configuration were measured using the Kelvin probe technique, with the ITO/NiO_x film set as the reference. Compared to this baseline, ITO/NiO_x/PVK and ITO/NiO_x/PFS-T-Li exhibited CPD shifts of −350 mV and −265 mV, respectively (Table S1), indicating downward energy level shifts of the surface Fermi level. This shift reflects the formation of interfacial dipoles and a modified electronic structure that promotes hole extraction. Although the CPD shift induced by PFS-T-Li is slightly smaller than that of PVK, the resulting energy level remains well aligned with the HOMO level of the perovskite (−6.3 eV), forming a cascade alignment across NiO_x, PFS-T-Li, and the perovskite layer (Fig. 1(c)). This favorable alignment, together with interfacial defect passivation, facilitates efficient hole injection and lowers the energetic barrier for charge transport.

To quantitatively assess the wettability and interfacial compatibility of ITO/NiO_x, ITO/NiO_x/PVK, and ITO/NiO_x/PFS-T-Li substrates with the perovskite precursor solution, contact angle measurements were performed using the actual precursor solution. This evaluation aimed to probe how effectively each interfacial layer promotes uniform spreading of the precursor and establishes favorable interfacial interactions. Among the tested surfaces, NiO_x/PFS-T-Li exhibited the lowest contact angle (10.60°), followed by NiO_x (26.68°) and NiO_x/PVK (42.24°) (Fig. 2(a)), indicating that PFS-T-Li delivers the highest degree of chemical com-

patibility with the perovskite solution. This improved affinity is attributed to the ionic and hydrophilic characteristics of the sulfonate side chains, which mitigate the interfacial energy mismatch at the NiO_x/perovskite interface.

To further investigate the intrinsic surface morphology of the underlying interlayers prior to perovskite deposition, atomic force microscopy (AFM) was conducted (Fig. 2(b)). The pristine NiO_x film exhibited a relatively high root-mean-square (R_q) roughness of 1.687 nm, arising from surface inhomogeneities such as oxygen vacancies and residual hydroxyl groups. Upon PVK deposition, the surface roughness decreased significantly to 1.149 nm due to the self-leveling nature of the polymeric film. However, given its non-polar and chemically inert character, PVK does not chemically interact with or passivate the NiO_x surface, as further reflected in its poor wettability with the perovskite solution.

In contrast, the NiO_x/PFS-T-Li surface displayed an intermediate R_q value of 1.448 nm, likely attributable to localized structural reorganization induced by electrostatic and coordination interactions between the sulfonate moieties and undercoordinated Ni sites. Notably, the concurrent decrease in contact angle and suppression of surface roughness-despite the absence of a purely smoothing polymer-provides indirect evidence that PFS-T-Li chemically mitigates the surface defect density of NiO_x. In particular, the coordination between sulfonate groups and NiO_x surface defects is

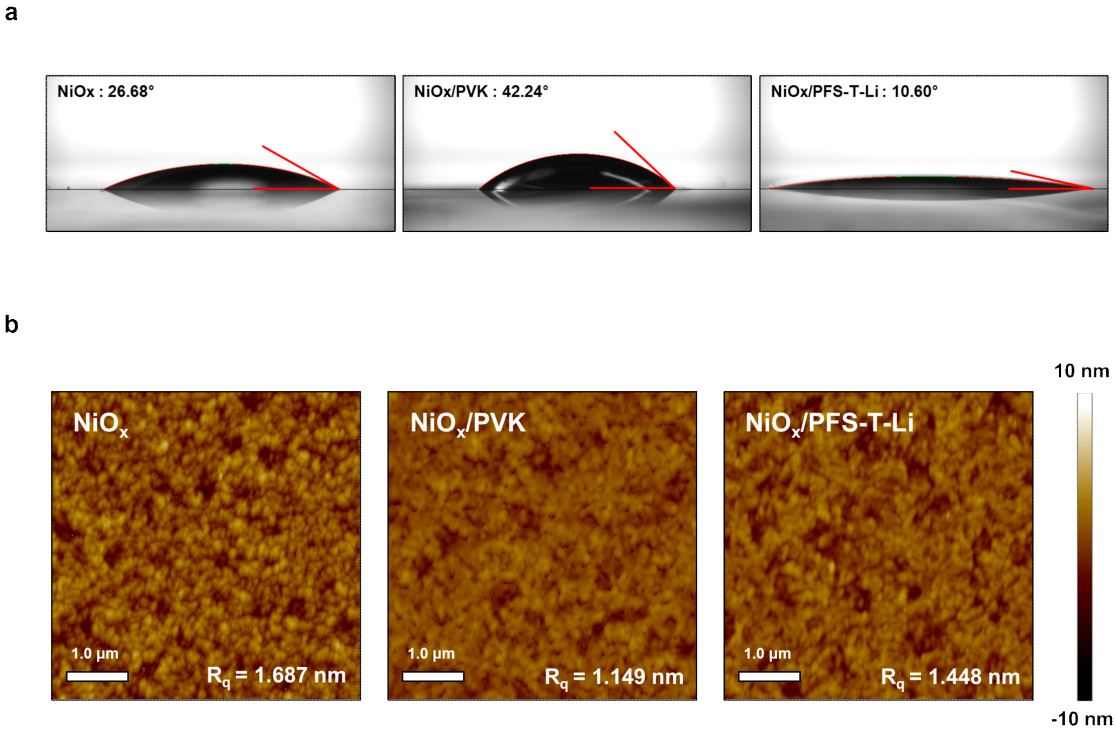

Fig. 2. Contact angle (a) and AFM analyses (b) of NiO_x-based interlayers for interfacial compatibility and surface defect modulation.

presumed to passivate oxygen vacancies, thereby reducing surface energy inhomogeneity and improving wetting behavior. These synergistic effects are critical for promoting uniform precursor film formation, facilitating nucleation, and ultimately enabling high-quality perovskite crystallization.

To elucidate the interfacial chemical environment, X-ray photoelectron spectroscopy (XPS) was conducted on quasi-2D perovskite films deposited on NiO_x and NiO_x/PFS-T-Li substrates (Fig 3. (a)−(c)). In the Cs 3d and Pb 4f core-level spectra, the NiO_x/PFS-T-Li sample exhibited discernible downshifts in binding energies by ~0.20 eV and ~0.25 eV, respectively, relative to the pristine NiO_x substrate. These shifts reflect a modified local electrostatic environment and reduced interfacial charge accumulation, likely arising from the ionic and coordinating nature of the sulfonate groups SO_3^- and Li^+ counterions, which selectively interact with undercoordinated Pb^{2+} sites and oxygen vacancies at the NiO_x interface. In the Ni 2p core-level spectra (Fig. 3(c)), the NiO_x/PFS-T-Li sample exhibited a slight downshift of ~0.05 eV in binding energy relative to the pristine NiO_x substrate. This shift suggests a subtle reduction in surface electrostatic interactions, likely due to passivation by the anionic sulfonate groups in PFS-T-Li.

Similarly, no significant shift was observed in the Br 3d spectra (Fig. S1), suggesting that halide ions, which are more tightly bound within the perovskite lattice, remain relatively unaffected by the interfacial modification. The element-specific nature of the observed chemical shifts underscores the selective passivation mechanism, wherein PFS-T-Li preferentially modulates the coordination environment of A-site (Cs^+) and B-site (Pb^{2+}) cations rather than lattice halides.

These interfacial interactions contribute to reduced trap-state density and improved charge distribution, supporting more favorable energy level alignment and enhanced optoelectronic performance in the subsequent device operation.

In the UV-Vis absorption spectra (Fig. 3(d)), distinct excitonic peaks at approximately 430 nm and 470 nm, corresponding to the n=1 and n=2 quasi-2D perovskite phases, were observed in all three configurations: NiO_x/perovskite, NiO_x/PVK/perovskite, and NiO_x/PFS-T-Li/perovskite. Notably, the peak intensities were substantially reduced in the NiO_x/ PFS- T-Li/perovskite sample, suggesting that the incorporation of PFS-T-Li suppresses the relative formation of low-n quasi-2D phases during crystallization. This suppression is attributed to the favorable interfacial environment provided by PFS-T-Li-particularly its ionic sulfonate moieties, which enhance surface wettability and modulate interfacial energetics, thereby directing the growth toward higher-n or more 3D-like perovskite domains. X-ray diffraction (XRD) analysis was conducted to further validate the phase evolution during crystallization (Fig. S2). The peaks at 15° and 30.5° correspond to the (100) and (200) planes of the $CsPbBr_3$ cubic phase, respectively, with the NiO_x/PFS-T-Li/perovskite films exhibiting the highest intensities among all samples. Such enhancement in these main perovskite reflections indicates improved crystallinity, which is attributed to an increased proportion of higher -n phases. The growth of these high-n phases implies a concurrent suppression of low-n phases, leading to a phase distribution shift toward more thermodynami-

cally stable crystal domains [43,44].

This morphological modulation is further supported by photoluminescence (PL) measurements (Fig. 3(e)). The NiO_x/PFS-T-Li-based film exhibited the strongest

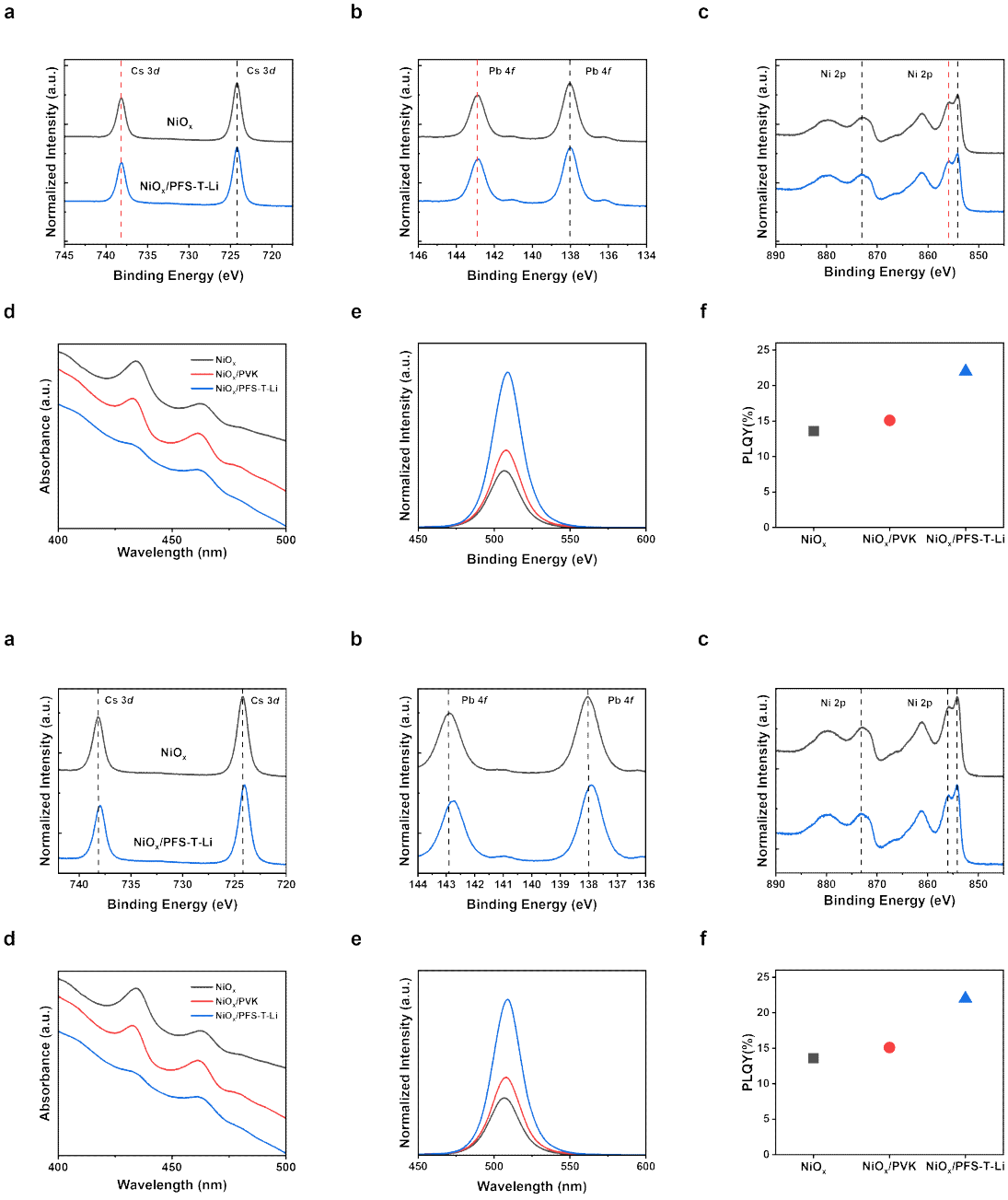

Fig. 3. X-ray photoelectron spectroscopy spectra of (a) Cs 3d, (b) Pb 4f, (c) Ni 2p. (d) UV–vis absorption spectra, (e) PL spectra, and (f) Photoluminescence quantum yield (PLQY) of quasi-2D perovskite films deposited on different HTLs (NiO_x, NiO_x/PVK, and NiO_x/PFS-T-Li).

PL intensity among the three configurations, indicating reduced non-radiative recombination losses and enhanced optoelectronic quality. Complementary photoluminescence quantum yield (PLQY) measurements (Fig. 3(f)) revealed a value of 22% for the NiO_x/PFS-T-Li film, representing a significant enhancement over NiO_x (13.6%) and NiO_x/PVK (15.1%). This finding supports our UV-vis absorption results (Fig. 3d) and is consistent with previous reports showing that reduced low-n phase content improves energy funneling and enhances PL emission efficiency in quasi-2D perovskites [43].

These findings collectively point to a synergistic interfacial passivation effect in the NiO_x/PFS-T-Li architecture, where Li^+ and SO_3^- groups selectively interact with Pb^{2+}-related defects in the perovskite and oxygen vacancies in the NiO_x, respectively. This dual-passivation mechanism not only mitigates trap-assisted recombination but also promotes more uniform and stable perovskite crystallization. As a result, both the optical emission characteristics and the underlying crystallographic phase distribution are simultaneously improved, laying the foundation for efficient and stable PeLED performance.

To investigate the impact of interfacial engineering on device performance, quasi-2D PeLEDs were fabricated using the structure ITO/HTLs (NiO_x, NiO_x/PVK, or NiO_x/PFS-T-Li)/perovskite/TPBi/LiF/Al, as illustrated in Fig. 4(a). This device architecture was designed to systematically evaluate how interfacial modifications influence charge injection, recombination dynamics, and overall optoelectronic characteristics. As

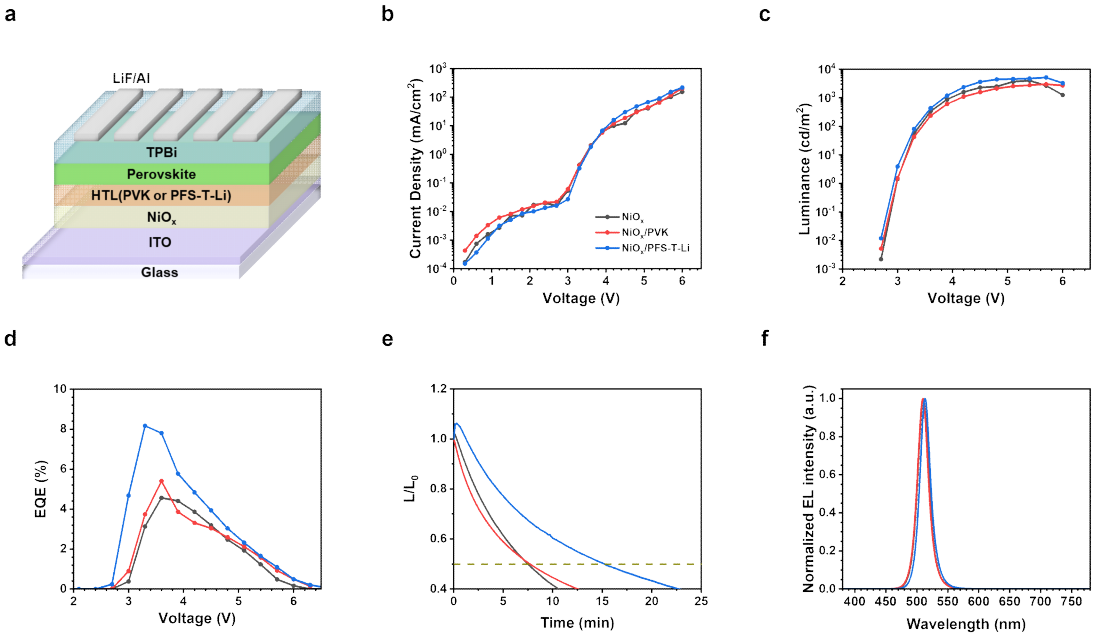

Fig. 4. (a) Device architecture of PeLED. (b) Current density-voltage (J–V) curves, (c) Luminance-voltage (L–V) curves, (d) *EQE-V* of PeLEDs with different HTLs. (e) Device stability measurement (T_{50}) with initial luminance of 100 c dm^{-2}. (f) Normalized electroluminescence spectra of each PeLEDs.

shown in the current density-voltage (J–V) characteristics (Fig. 4(b)), all devices exhibited typical diode-like behavior. Notably, the NiO_x/PFS-T-Li-based device showed a relatively lower current density in the low-bias region (under 3 V), suggesting suppressed leakage current, likely due to effective defect passivation by the sulfonate-functionalized PFS-T-Li layer. At higher voltages within the operational regime, the same device exhibited a markedly higher current density compared to the control (NiO_x) and PVK-based devices. This improvement reflects more efficient hole injection, which can be attributed to favorable energy level alignment at the NiO_x/PFS-T-Li/perovskite interface and improved interfacial crystallinity, resulting in minimized energetic barriers for carrier transport.

The luminance-voltage (L–V) characteristics (Fig. 4(c)) further support this trend. The device incorporating PFS-T-Li exhibited the highest peak luminance of 5,111 cd m^{-2}, compared to 4,153 cd m^{-2} and 3,735 cd m^{-2} for the PVK and bare NiO_x devices, respectively. These improvements are consistent with suppressed non-radiative recombination and more balanced carrier injection, resulting from the dual-passivation effects of PFS-T-Li at both the NiO_x and perovskite interfaces.

Notably, the device with the PFS-T-Li interlayer also exhibited the highest external quantum efficiency (EQE), reaching 8.16% at 3.3 V (Fig. 4(d)). In comparison, devices with PVK and bare NiO_x reached peak EQEs of 5.59% and 4.14%, respectively, at higher voltages. The enhanced performance is attributed to the combined benefits of reduced trap-assisted recombination, improved perovskite film morphology, and better energy level alignment achieved through PFS-T-Li incorporation. The quantitative performance metrics are summarized in Table S2.

Operational stability was evaluated by monitoring the time to 50% initial luminance (T_{50}) under continuous operation at 100 cd m^{-2} (Fig. 4(e)). The PFS-T-Li-based device exhibited a T_{50} of 15.2 minutes, approximately double that of the PVK (7.7 minutes) and NiO_x (7.5 minutes) devices, underscoring the stabilizing effect of interfacial passivation on device degradation.

Electroluminescence (EL) spectra from all devices exhibited sharp green emission with FWHM values consistently below 20 nm, indicating high color purity regardless of the interfacial layer used. The NiO_x and NiO_x/PVK-based devices showed peak emission at 510 nm, while the NiO_x/PFS-T-Li-based device exhibited peak emission at 513 nm, maintaining emission within the green spectral range.

4. CONCLUSION

In summary, we report a multifunctional interfacial engineering strategy for PeLEDs using an anionic conjugated polyelectrolyte, PFS-T-Li, as an interfacial layer on NiO_x-based hole transport layers. The π-conjugated fluorene-thiophene backbone facilitates hole transport, while the sulfonate and lithium moieties simultaneously passivate oxygen vacancies in NiO_x and Pb^{2+}-related defects in the perovskite layer. This dual-passivation mechanism improves interfacial compatibility, suppresses non-radiative recombination, and promotes uniform perovskite crystallization. Consequently, devices incorporating the NiO_x/PFS-T-Li interlayer exhibit significantly enhanced external quantum efficiency (8.16%) and luminance (5,111 cd m^{-2}),

along with improved operational stability. These findings demonstrate the efficacy of PFS-T-Li as an interfacial modulator, offering a viable pathway toward efficient and stable PeLEDs.

ABBREVIATIONS

PeLEDs: Perovskite light-emitting diodes
NiO_x: Nickel oxide
CPE: Conjugated polyelectrolyte
PFS-T-Li: Poly[9,9-bis(4-C-sulfonatobutyl)fluorene-alt-thiophene]-Li
HTL: Hole transport layer
FWHM: Full width at half maximum
PVK: Poly(9-vinylcarbazole)
DMSO: Dimethyl sulfoxide
CB: Chlorobenzene
TPBi: 2,2′,2″-(1,3,5-Benzinetriyl)-tris(1-phenyl-1-H-benzimidazole)
LiF: Lithium fluoride
ITO: Indium tin oxide
KPM: Kelvin probe microscopy
CPD: Contact potential difference
AFM: Atomic force microscopy
R_q: Root mean square roughness
XPS: X-ray photoelectron spectroscopy
PL: Photoluminescence
PLQY: Photoluminescence quantum yield
UV-Vis: Ultraviolet-visible spectroscopy
XRD: X-ray diffraction
EL: Electroluminescence
EQE: External quantum efficiency
T_{50}: Time to 50% initial luminance

ACKNOWLEDGMENTS

Author Contributions

BCP, HY, JHK and BRL initiated the project. RFBN synthesized the CPE, and DHS performed the characterization of the CPE. BCP and JK performed formal analysis and device fabrication under supervision of BRL. BCP, HSY drafted the first version of the manuscript, and JHK, HY, BRL revised it. All the authors have contributed to the manuscript.

Funding

This work was supported by the National Research Foundation of Korea (NRF) grant funded by the Korean government (RS-2024-00462833). This work was supported by a Korea Basic Science Institute (National research Facilities and Equipment Center) grant funded by the Ministry of Education (RS-2025-02308784).

Declarations of Competing Interests

The authors declare that they have no competing interests.

REFERENCES

[1] Hassan, Y.; Park, J. H.; Crawford, M. L.; Sadhanala, A.; Lee, J.; Choi, S. J. et al. Ligand-Engineered Bandgap Stability in Mixed-Halide Perovskite LEDs. Nature 2021, 591 (7848), 72-77.

[2] Li, M., Yang, Y., Kuang, Z., Hao, C., Wang, S., Lu, F. et al. (2024). Acceleration of radiative recombination for efficient Perovskite LEDs. Nature,

630(8017), 631-635.

[3] Fakharuddin, A.; Gangishetty, M. K.; Abdi-Jalebi, M.; Chin, S. H.; bin Mohd Yusoff, A. R.; Congreve, D. N. et al. Perovskite Light-Emitting Diodes. Nat. Electron. 2022, 5 (4), 203-216.

[4] Han, T. H.; Jang, K. Y.; Dong, Y.; Friend, R. H.; Sargent, E. H.; Lee, T. W. A Roadmap for the Commercialization of Perovskite Light Emitters. Nat. Rev. Mater. 2022, 7 (10), 757-777.

[5] Quan, L. N.; Rand, B. P.; Friend, R. H.; Mhaisalkar, S. G.; Lee, T. W.; Sargent, E. H. Perovskites for Next-Generation Optical Sources. Chem. Rev. 2019, 119 (12), 7444-7477.

[6] Cho, H.; Jeong, S. H.; Park, M. H.; Kim, Y. H.; Wolf, C.; Lee, C. L. et al. Overcoming the Electroluminescence Efficiency Limitations of Perovskite Light-Emitting Diodes. Science 2015, 350 (6265), 1222-1225.

[7] Shen, X.; Kang, K.; Yu, Z.; Jeong, W. H.; Choi, H.; Park, S. H. et al. Passivation Strategies for Mitigating Defect Challenges in Halide Perovskite Light-Emitting Diodes. Joule 2023, 7 (2), 272-308.

[8] Lee, A.; Kim, J.; Jeong, W. H.; Park, J. H.; Kim, D.; Huang, C. S. et al. Mitigating Bulk Halide Defects in Blue-Emissive Perovskite Nanocrystals Using Benzoyl Halides for Efficient Light-Emitting Diodes. Chem. Eng. J. 2024, 500, 157198.

[9] Ramadan, A. J.; Jeong, W. H.; Oliver, R. D. J.; Jiang, J.; Dasgupta, A.; Yuan, Z. et al. The Role of the Organic Cation in Developing Efficient Green Perovskite LEDs Based on Quasi-2D Perovskite Heterostructures. Adv. Funct. Mater. 2024, 34 (14), 2309653.

[10] Yu, Z.; Shen, X.; Fan, X.; Jung, Y. K.; Jeong, W. H.; Dasgupta, A. et al. Hydrogen Bond-Assisted Dual Passivation for Blue Perovskite Light-Emitting Diodes. ACS Energy Lett. 2023, 8 (10), 4296-4303.

[11] Song, H.; Yang, J.; Jeong, W. H.; Lee, J.; Lee, T. H.; Yoon, J. W. et al. A Universal Perovskite Nanocrystal Ink for High Performance Optoelectronic Devices. Adv. Mater. 2023, 35 (8), 2209486.

[12] Jeong, W. H.; Yu, Z.; Gregori, L.; Yang, J.; Ha, S. R.; Jang, J. W. et al. *In Situ* Cadmium Surface Passivation of Perovskite Nanocrystals for Blue LEDs. J. Mater. Chem. A 2021, 9 (47), 26750-26757.

[13] Kim, G. Y.; Jung, C. W.; Chin, S. H.; Jeong, W. H.; Lee, B. R.; Kim, J. H. et al. Controlled Phase Distribution of Quasi-2D Perovskite Enables Improved Electroluminescence. J. Phys. Energy 2024, 6 (3), 035002.

[14] Zhou, W.; Shen, Y.; Cao, L. X.; Lu, Y.; Tang, Y. Y.; Zhang, K. et al. High Efficiency Perovskite Polymer Bulk Heterostructure Light Emitting Diodes. Nat. Photonics 2018, 12 (12), 783-789.

[15] Zhou, W.; Shen, Y.; Cao, L. X.; Lu, Y.; Tang, Y. Y.; Zhang, K. et al. Manipulating Ionic Behavior with Bifunctional Additives for Efficient Sky Blue Perovskite Light Emitting Diodes. Adv. Funct. Mater. 2023, 33 (27), 2301425.

[16] Jeong, W. H.; Lee, S.; Song, H.; Shen, X.; Choi, H.; Choi, Y. et al. Synergistic Surface Modification for High Efficiency Perovskite Nanocrystal Light Emitting Diodes: Divalent Metal Ion Doping and Halide-Based Ligand Passivation. Adv. Sci. 2024, 11 (4), 2305383.

[17] Yu, Z.; Ha, S. R.; Park, J. H.; Jung, E. D.; Jeong, W. H.; Kim, S. et al. Water-Stable Polymer Hole Transport Layer in Organic and Perovskite Light-Emitting Diodes. J. Power Sources 2020, 478, 228810.

[18] Lee, D. H.; Jeong, W. H.; Choung, S.; Jang, J. W.; Lee, G.; Song, H. et al. Surface Defect Recovery in Perovskite Nanocrystals with Excess Halide for Core-Shell Structure. ACS Energy Lett. 2024, 9 (11), 5413-5420.

[19] Han, S.; Jeong, W. H.; Seo, G.; Choi, S.; Lee, D. G.; Chae, W. S. et al. Synergistic Hybrid Ligand Passivation of Perovskite Quantum Dots: Suppressing Reduced Dimensionality and Enhancing Optoelectronic Performance. Adv. Mater. 2025, 2410128.

[20] Wan, Q.; Zheng, W.; Zou, C.; Carulli, F.; Zhang, C.; Song, H. et al. Ultrathin Light-Emitting Diodes with External Efficiency over 26% Based on Resurfaced Perovskite Nanocrystals. ACS Energy Lett. 2023, 8, 927-934.

[21] Mahmoudi, T.; Wang, Y.; Hahn, Y. B. Highly Stable Perovskite Solar Cells Based on Perovskite /NiO-Graphene Composites and NiO Interface with 25.9 mA/cm² Photocurrent Density and 20.8% Efficiency. Nano Energy 2021, 79, 105452.

[22] Kim, T.; Lee, M. H. Display Application and Development Trend of Perovskite Emitters. J. Flex. Print. Electron. 2022, 1(1), 13-28.

[23] Fan, X.; Wang, Y.; Shen, X.; Yu, Z.; Jung, W. H.; Jang, J. W. et al. Phosphine Oxide Modulator-Ameliorated Hole Injection for Blue Perovskite Light-Emitting Diodes. J. Mater. Chem. A 2023, 11 (38), 20808-20815.

[24] Yu, Z.; Jeong, W. H.; Kang, K.; Song, H.; Shen, X.; Ahn, H. et al. A Polymer/Small-Molecule Binary-Blend Hole Transport Layer for Enhancing Charge Balance in Blue Perovskite Light Emitting Diodes. J. Mater. Chem. A 2022, 10 (26), 13928-13935.

[25] Yu, X.; Liu, C.; Li, C.; Wang, C.; Li, Y.; Liang, L. et al. Controlled NiO_x Defect Engineering to Harness Redox Reactions in Perovskite Photovoltaic Cells via Atomic Layer Deposition. ACS Appl. Mater. Interfaces 2024, 16 (24), 31114-31125.

[26] Du, X.; Li, F.; Li, Y.; Xia, H.; Yang, E.; Ahn, Y. et al. Efficient Functional Compensation Layer Integrated with HTL for Improved Stability and Performance in Perovskite Solar Cells. Small 2025, 2410369.

[27] Boyd, C. C.; Shallcross, R. C.; Moot, T.; Kerner, R.; Bertoluzzi, L.; Onno, A. et al. Overcoming Redox Reactions at Perovskite-Nickel Oxide Interfaces to Boost Voltages in Perovskite Solar Cells. Joule 2020, 4 (8), 1759-1775.

[28] Liu, Y.; Long, B.; Chen, R.; Huang, S.; Ou-Yang, W.; Chen, X. Enhanced Efficiency and Stability of NiO_x-Based Perovskite Solar Cells Using [6,6]-Phenyl-C61-Butyric Acid Methyl-Doped Poly (9-Vinylcarbazole)-Modified Layer. ACS Appl. Energy Mater. 2021, 4 (4), 3812-3821.

[29] Liu, X.; Liu, Y.; Lang, R.; Liu, Y.; Lei, W.; Cong, R. et al. Optimizing the Performance of Sputtered-NiO_x-Based Perovskite Solar Cells via Regulating the PbI2 Concentration. Energy Technol. 2023, 11 (9), 2300355.

[30] Xie, J.; Li, D.; Li, H.; Peng, B.; Bao, Q.; Jiang,

J. et al. Surface and Bulk Defect Passivation in MAPbI3 Perovskites with Daminozide: Effects on Carrier Dynamics and Mobility. Adv. Sci. 2025, 2500530.

[31] Lee, H.; Lee, J. S.; Cho, H. Recent Advances in Template-Based Printing Techniques of Metal Halide Perovskites. J. Flex. Print. Electron. 2024, 3 (2), 131-143.

[32] Lee, S.; Nguyen, T. L.; Lee, S. Y.; Jang, C. H.; Lee, B. R.; Jung, E. D. et al. Conjugated Polyelectrolytes Bearing Various Ion Densities: Spontaneous Dipole Generation, Poling Induced Dipole Alignment, and Interfacial Energy Barrier Control for Optoelectronic Device Applications. Adv. Mater. 2018, 30 (14), 1706034.

[33] Zou, Y.; Ban, M.; Yang, Y.; Bai, S.; Wu, C.; Han, Y. et al. Boosting Perovskite Light-Emitting Diode Performance via Tailoring Interfacial Contact. ACS Appl. Mater. Interfaces 2018, 10 (28), 24320-24326.

[34] Ge, Z.; Wan, S.; Moin, M.; Moyez, S. A.; Dong, L.; Haris, H. R. et al. Boosting Electronic Properties of $CsPbBr_3$ Nanocrystals via Lithium Ion Doping and Surface Passivation for Enhanced Electrical Conductivity and Efficient White Light Emitting Diodes. Adv. Sci. 2025, 2417304.

[35] Nasrun, R. F. B.; Son, D. H.; Kim, J. H.; Kim, J. H. Water-Soluble Anionic Polymer Electrolytes Based on Polyfluorene as the Universal Interlayer for Organic Solar Cells. Macromol. Res. 2024, 1-8.

[36] Kim, J.; Nasrun, R. F. B.; Jeong, W. H.; Shen, X.; Sausan, I. S.; Kim, D. et al. Conjugated Polyelectrolytes as a Defect-Passivating Hole Injection Layer for Efficient and Stable Perovskite Light-Emitting Diodes. ACS Appl. Electron. Mater. 2024, 6(12), 8929-8937.

[37] Park, J. H.; Noh, Y. W.; Ha, J. M.; Harit, A. K.; Tripathi, A.; Lee, J. et al. Anionic Conjugated Polyelectrolyte as a Semiconducting Additive for Efficient and Stable Perovskite Solar Cells. ACS Appl. Mater. Interfaces 2023, 16 (16), 19937-19946.

[38] Lee, S.; Kim, D. B.; Yu, J. C.; Jang, C. H.; Park, J. H.; Lee, B. R. et al. Versatile Defect Passivation Methods for Metal Halide Perovskite Materials and Their Application to Light Emitting Devices. Adv. Mater. 2019, 31(20), 1805244.

[39] He, Q.; Zhang, Z.; Chen, A.; Zhang, T.; Chen, X.; Bian, X. et al. Surface Passivation with an Electron-Donating Sulfonate Group for High-Performance and Stable Perovskite Solar Cells. J. Mater. Chem. A 2024, 12(21), 12545-12551.

[40] Liu, Y.; Xu, T.; Xu, Z.; Zhang, H.; Yang, T.; Wang, Z. et al. Defect Passivation and Lithium Ion Coordination via Hole Transporting Layer Modification for High Performance Inorganic Perovskite Solar Cells. Adv. Mater. 2024, 36 (4), 2306982.

[41] Wang, H.; Zou, W.; Luo, H.; Quan, Y.; Yang, L.; Liu, X. et al. Ion Migration Inhibition and Defect Passivation via Sulfonate Salt Coordination for High-Performance Perovskite Solar Cells with Enhanced Phase Stability. J. Mater. Chem. C 2023, 11 (39), 13518-13525.

[42] He, Q.; Zhang, Z.; Chen, A.; Zhang, T.; Chen, X.; Bian, X. et al. Surface Passivation with an Electron-Donating Sulfonate Group for High-

Performance and Stable Perovskite Solar Cells. J. Mater. Chem. A 2024, 12 (21), 12545-12551.

[43] Liu, Y.; Yu, Z.; Chen, S.; Park, J. H.; Jung, E. D.; Lee, S. et al. Boosting the Efficiency of Quasi-2D Perovskites Light-Emitting Diodes by Using Encapsulation Growth Method. Nano Energy 2021, 80, 105511.

[44] Li, F.; Zhang, X.; Wang, Y.; Chen, J.; Liu, H.; Zhao, Q. et al. Enhancing Energy Transfer through Structure Reconstruction of Quasi-2D Perovskites for Highly Efficient Light-Emitting Diodes. ACS Mater. Lett. 2024, 6 (4), 1484-1490.